Modeling evolution of dark matter substructure and annihilation boost

Hiroshima, N.; Ando, S.; Ishiyama, T.

DOI
10.1103/PhysRevD.97.123002
Publication date
2018
Document Version
Final published version
Published in
Physical Review D. Particles, Fields, Gravitation, and Cosmology

Modeling evolution of dark matter substructure and annihilation boost

Nagisa Hiroshima,[1,2] Shin'ichiro Ando,[3,4] and Tomoaki Ishiyama[5]

[1]*Institute for Cosmic Ray Research, University of Tokyo, Kashiwa, Chiba 277-8582, Japan*
[2]*Institute of Particle and Nuclear Studies, High Energy Accelerator Research Organization (KEK), Tsukuba, Ibaraki 305-0801, Japan*
[3]*GRAPPA Institute, Institute of Physics, University of Amsterdam, 1098 XH Amsterdam, The Netherlands*
[4]*Kavli Institute for the Physics and Mathematics of the Universe (Kavli IPMU, WPI), Todai Institutes for Advanced Study, University of Tokyo, Kashiwa, Chiba 277-8583, Japan*
[5]*Institute of Management and Information Technologies, Chiba University, Chiba 263-8522, Japan*

(Received 28 March 2018; published 8 June 2018)

We study evolution of dark matter substructures, especially how they lose mass and change density profile after they fall in gravitational potential of larger host halos. We develop an analytical prescription that models the subhalo mass evolution and calibrate it to results of N-body numerical simulations of various scales from very small (Earth size) to large (galaxies to clusters) halos. We then combine the results with halo accretion histories and calculate the subhalo mass function that is physically motivated down to Earth-mass scales. Our results—valid for arbitrary host masses and redshifts—have reasonable agreement with those of numerical simulations at resolved scales. Our analytical model also enables self-consistent calculations of the boost factor of dark matter annihilation, which we find to increase from tens of percent at the smallest (Earth) and intermediate (dwarfs) masses to a factor of several at galaxy size, and to become as large as a factor of $\sim$10 for the largest halos (clusters) at small redshifts. Our analytical approach can accommodate substructures in the subhalos (sub-subhalos) in a consistent framework, which we find to give up to a factor of a few enhancements to the annihilation boost. The presence of the subhalos enhances the intensity of the isotropic gamma-ray background by a factor of a few, and as the result, the measurement by the Fermi Large Area Telescope excludes the annihilation cross section greater than $\sim 4 \times 10^{-26}$ cm^3 s^{-1} for dark matter masses up to $\sim$200 GeV.

DOI: 10.1103/PhysRevD.97.123002

I. INTRODUCTION

There is strong evidence for the existence of dark matter, such as the distribution of matter in the Universe [1,2], rotation curves of galaxies [3,4], and bullet clusters [5]. In spite of the efforts to unveil the nature of the dark matter, however, our knowledge about it is still limited. Many models of particle dark matter have been proposed, and among them, weakly interacting massive particles (WIMPs) are one of the best studied in accordance with supersymmetric extensions of the standard model [6]. If dark matter is made of new particles such as WIMPs, which have a small but finite interaction with the standard model sector, we expect them to be detected through the observations of gamma rays from self-annihilation of dark matter particles [7].

Dark matter forms virialized objects—dark matter halos, which give some hints about its nature. For example, they encode information of scattering between dark matter particles and the standard model particles in the early Universe, through the minimum halo mass being predicted to be 10^{-12}–10^{-3} $M_\odot$ for the supersymmetric neutralino [8–11]. Halos grow larger and larger by merging with each other and accreting smaller ones, leaving imprints of dark matter properties in their hierarchical structures. Smaller halos that are accreted onto larger (host) halos are referred to as subhalos or substructures. Once subhalos are trapped by their hosts, they lose their mass through a gravitational tidal force while orbiting. With given properties of the host and subhalos at their accretion, we can determine the tidal mass loss of the subhalos and remaining structures after some orbiting time. This procedure is studied through the analytical [12–14], semianalytical [15], and numerical [16–21] approaches.

Subhalos remaining in their host are *boosters* for indirect detection experiments of particle dark matter [22–27], especially for gamma-ray telescopes such as the Fermi Large Area Telescope (LAT). In order to discuss the evolution of subhalo abundance, mass distribution, and density profile, and to estimate the substructure boost, analytical modeling is a powerful tool since they do not suffer from resolution limits. We can cover a wide range of magnitude in both the host-halo mass and the mass ratio of the hosts to subhalos in the analytical calculations.

In this paper, we discuss properties of subhalos after tidal stripping and, as one of the applications, the boost factor for the gamma-ray signals from dark matter annihilation.

This study updates calculations of the substructure boost by Ref. [27] in various aspects. In order to access the properties of the subhalos after accretion, we follow an analytical approach in Ref. [14], which considers the mass loss of the subhalos due to the tidal stripping under the potential of the host halos. This analytical model is physically motivated although it has simplified some aspects of tidal stripping. We include the host mass and redshift dependence of the tidal stripping for the purpose of improving the accuracy of the models. Then, we consistently take evolutions of the host and subhalos into account in calculations of their properties. After modeling of the tidal mass loss of subhalos, we calculate the boost factors of the subhalos for the gamma-ray signals from dark matter annihilation as well as the mass function of subhalos.

The structure of this article is as follows. In Sec. II, we explain the ways to derive the properties of subhalos after tidal stripping from quantities at the accretion time. In Sec. III, we derive the host mass and redshift dependence of the subhalo mass-loss rate. In Sec. IV, we show applications to the observational signatures such as the subhalo mass function and annihilation boost factor. We then discuss implications for the isotropic gamma-ray background in Sec. V and summarize our findings in Sec. VI. Throughout the paper, we adopt cosmological parameters from Ref. [2] (Table 4, "TT+lowP +lensing"), and use "ln" and "log" to represent natural and 10-base logarithmic functions, respectively.

II. DENSITY PROFILE OF SUBHALOS

Dark matter halos have evolved by merging and accretion. After accretion onto their hosts, subhalos lose their mass due to tidal stripping while they are orbiting in their host's gravitational potential. In this section, we show that the properties of subhalos after tidal stripping can be determined given the mass $m_{\rm acc}$ at accretion redshift $z_{\rm acc}$ for given host halos, on a statistical basis. Starting from $(m_{\rm acc}, z_{\rm acc})$, we can calculate the subhalo mass at a redshift z_0, denoted as m_0, by integrating its mass-loss rate $\dot{m}$ from accretion redshift $z_{\rm acc}$ to z_0. We parametrize the mass-loss rate as

$$\dot{m}(z) = -A\frac{m(z)}{\tau_{\rm dyn}(z)}\left[\frac{m(z)}{M(z)}\right]^{\zeta}, \tag{1}$$

where $\tau_{\rm dyn}(z)$ is the dynamical time scale [14]. The evolution of the host mass $M(z)$ is discussed in Ref. [28], and is also summarized in Appendix A. Parameters A and ζ are taken to be constants in Ref. [14], but in a more realistic case, both of them should depend on the host mass $M(z)$ and the redshift z. We derive the dependence following the analytical discussion in Ref. [14] with several updates in the next section.

In this section, we show how density profiles of the subhalos including a scale radius r_s and a characteristic density ρ_s evolve, associated with the evolution of the subhalo mass from $m_{\rm acc}$ at $z_{\rm acc}$ to m_0 at z_0. Throughout our calculations, we adopt the Navarro-Frenk-White (NFW) density profile [29] up to a truncation radius r_t, and zero beyond:

$$\rho(r) = \begin{cases} \rho_s r_s^3/[r(r+r_s)^2], & \text{for } r \le r_t, \\ 0, & \text{for } r > r_t. \end{cases} \tag{2}$$

First, we determine ρ_s and r_s at the accretion redshift $z_{\rm acc}$. As it was a *field* halo (i.e., a halo that is not in a larger halo's gravitational potential) when accreted, we first determine the virial radius $r_{\rm vir,acc}$ at $z_{\rm acc}$ from the mass of the subhalo at accretion $m_{\rm acc}$,

$$m_{\rm acc} = \frac{4\pi}{3}\Delta_c(z_a)\rho_c(z_{\rm acc})r_{\rm vir,acc}^3, \tag{3}$$

where $\Delta_c = 18\pi^2 + 82d - 39d^2$, $d = \Omega_m(1+z_{\rm acc})^3/[\Omega_m(1+z_{\rm acc})^3 + \Omega_\Lambda] - 1$ [30], and $\rho_c(z_{\rm acc})$ is the critical density at $z_{\rm acc}$. The scale radius is determined by $r_{s,\rm acc} = r_{\rm vir,acc}/c_{\rm vir,acc}$ at $z_{\rm acc}$ once a concentration parameter $c_{\rm vir,acc}$ is given. The concentration follows the log-normal distribution, whose mean is obtained in, e.g., Ref. [31], which is summarized in Appendix B. Note that Ref. [31] defines the concentration as a function of halo masses measured in M_{200}, defined as an enclosed mass in a radius within which the average density is 200 times the critical density. The virial concentration parameter $c_{\rm vir,acc}$ is obtained by a conversion between different definitions of mass [32], followed by $c_{\rm vir,acc} = c_{200,\rm acc}r_{\rm vir,acc}/r_{200,\rm acc}$. For the rms of the log-normal distribution, we adopt $\sigma_{\log c} = 0.13$ [33]. The characteristic density $\rho_{s,\rm acc}$ is then determined from

$$\rho_{s,\rm acc} = \frac{m_{\rm acc}}{4\pi r_{s,\rm acc}^3 f(c_{\rm vir,acc})}, \tag{4}$$

where

$$f(c) = \ln(1+c) - \frac{c}{1+c}. \tag{5}$$

The set of parameters $(r_{s,\rm acc}, \rho_{s,\rm acc})$ is related to the maximum circular velocity $V_{\rm max}$ and radius $r_{\rm max}$ at which the circular velocity reaches the maximum through

$$r_s = \frac{r_{\rm max}}{2.163}, \tag{6}$$

$$\rho_s = \frac{4.625}{4\pi G}\left(\frac{V_{\rm max}}{r_s}\right)^2. \tag{7}$$

Reference [34] derived the relation between the subhalo properties before and after the tidal stripping by following the evolution of $V_{\rm max}$ and $r_{\rm max}$. The relation between the $(V_{\rm max}, r_{\rm max})$ at accretion redshift $z_{\rm acc}$ and those at the arbitrarily chosen observation redshift z_0, in terms of the mass ratio after and before tidal stripping $m_0/m_{\rm acc}$, is

$$\frac{V_{\rm max,0}}{V_{\rm max,acc}} = \frac{2^{0.4}(m_0/m_{\rm acc})^{0.3}}{(1+m_0/m_{\rm acc})^{0.4}}, \tag{8}$$

$$\frac{r_{\rm max,0}}{r_{\rm max,acc}} = \frac{2^{-0.3}(m_0/m_{\rm acc})^{0.4}}{(1+m_0/m_{\rm acc})^{-0.3}}, \tag{9}$$

for the inner density profile proportional to r^{-1}, as is the case of the NFW. Then, we can determine $r_{s,0}$ and $\rho_{s,0}$ at $z = z_0$ through $V_{\rm max}$ and $r_{\rm max}$ in Eqs. (6) and (7). Finally, the truncation radius $r_{t,0}$ is determined from m_0, $\rho_{s,0}$, and $r_{s,0}$ by solving

$$m_0 = 4\pi\rho_{s,0}r_{s,0}^3 f\left(\frac{r_{t,0}}{r_{s,0}}\right). \tag{10}$$

We remove the subhalos with $r_{t,0}/r_{s,0} < 0.77$ from further consideration, as it is usually assumed that the subhalos satisfying this condition are completely disrupted [35]. (But see Ref. [21] for a claim otherwise.)

To summarize, following the prescription in this section (and the mass-loss rate $\dot{m}$ discussed in the next section), we can determine the density profile of the subhalos after tidal stripping at an arbitrary redshift z_0 up to scatter of the concentration-mass relation, given the mass and redshift of accretion, $m_{\rm acc}$ and $z_{\rm acc}$. Combined with the distribution of $m_{\rm acc}$ and $z_{\rm acc}$ that is obtained with the extended Press-Schechter formalism [36] (summarized in Appendix C), we can compute the statistical average of subhalo quantities of various interests. Among them, we discuss the subhalo mass functions and annihilation boost factor in Sec. IV.

III. TIDAL STRIPPING

The subhalo mass-loss rate $\dot{m}$, as can be seen in Eq. (1), should depend on both the redshift z and the host mass $M(z)$, since the subhalo evolution is determined by the tidal force of their host. Following Ref. [14], by assuming that tidal stripping of the subhalos occurs in one complete orbital period and there are no lags between the subhalo accretion and the tidal stripping of those accreted, we estimate the mass-loss rate of the accreted subhalos on a certain host at any redshift in an analytical way. We also show consistency of our results with those obtained by numerical simulations.

A. Analytical model

The mass loss $\dot{m}(z)$ of any subhalo is approximated as

$$\dot{m} = \frac{m - m(r_t)}{T_r}, \tag{11}$$

where T_r, m, and $m(r_t)$ are the orbital period, the virial mass of the subhalo just after accretion, and the mass enclosed in the tidal truncation radius r_t of the subhalo, respectively. In order to determine the orbit of the subhalo, we draw the orbit circularity η at infall and the radius of the circular orbit R_c from distribution functions for each parameter:

$$P(R_c) = \begin{cases} 5/2 & (0.6 \le R_c/R_{\rm vir} \le 1.0), \\ 0 & (\text{otherwise}), \end{cases} \tag{12}$$

$$P(\eta) = C_0(M,z)\eta^{1.05}(1-\eta)^{C_1(M,z)}, \tag{13}$$

where

$$C_0 = 3.38\left(1 + 0.567\left[\frac{M}{M_*(z)}\right]^{0.152}\right), \tag{14}$$

$$C_1 = 0.242\left(1 + 2.36\left[\frac{M}{M_*(z)}\right]^{0.107}\right), \tag{15}$$

$$\log\left[\frac{M_*(z)}{h^{-1}\,M_\odot}\right] = 12.42 - 1.56z + 0.038z^2. \tag{16}$$

We note that Eqs. (13)–(16) are calibrated with simulations up to $z = 7$ [37]. Pairs of η and R_c correspond to the pairs of the angular momentum L and the total energy E of the orbiting subhalo as follows:

$$E = \frac{1}{2}V_c^2 + \Phi(R_c), \tag{17}$$

$$L = \eta R_c V_c, \tag{18}$$

where $V_c = (GM/R_c)^{1/2}$ is a velocity at the circular orbit. The gravitational potential of the host Φ is

$$\Phi(R) = -V_{\rm vir}^2 \frac{\ln[1 + c_{\rm vir}^{\rm host} R/R_{\rm vir}]}{f(c_{\rm vir}^{\rm host})R/R_{\rm vir}}, \tag{19}$$

with $V_{\rm vir} = (GM/R_{\rm vir})^{1/2}$ and $c_{\rm vir}^{\rm host}$ the host halo's virial velocity and virial concentration, respectively. Here, we draw $c_{\rm vir}^{\rm host}$ from the log-normal distribution as discussed in the previous section.

Next, we determine the orbital period, T_r, and the truncation radius of the subhalo, r_t. They are derived from the pericenter radius R_p and the apocenter radius R_a, which are obtained by solving

$$\frac{1}{R^2} + \frac{2[\Phi(R) - E]}{L^2} = 0. \tag{20}$$

The orbital period T_r is then

$$T_r = 2\int_{R_p}^{R_a} \frac{dR}{\sqrt{2[E - \Phi(R)] - L^2/R^2}}. \tag{21}$$

The truncation radius r_t is obtained by solving the equation

TABLE I. Details of five cosmological N-body simulations used in this study. Here, N, L, and $m_{\rm p}$ are the total number of particles, box size, and mass of a simulation particle, respectively.

Name	N	L	Softening	$m_{\rm p}$ [$M_\odot$]	Reference
ν^2GC-S	2048^3	411.8 Mpc	6.28 kpc	3.2×10^8	[38,40]
ν^2GC-H2	2048^3	102.9 Mpc	1.57 kpc	5.1×10^6	[38,40]
Phi-1	2048^3	47.1 Mpc	706 pc	4.8×10^5	Ishiyama *et al.* (in prep)
Phi-2	2048^3	1.47 Mpc	11 pc	14.7	Ishiyama *et al.* (in prep)
A_N8192L800	8192^3	800.0 pc	2.0×10^{-4} pc	3.7×10^{-11}	Ishiyama *et al.* (in prep)

$$r_t = R_p \left[\frac{m(r_t)/M(<R_p)}{2 + \frac{L^2}{R_p GM(<R_p)} - \left.\frac{d\ln M}{d\ln R}\right|_{R_p}} \right]^{\frac{1}{3}}. \quad (22)$$

Assuming that ρ_s and r_s hardly change as the result of one complete orbit after the infall, we specify the mass profile $m(r)$ up to truncation radius r_t, and hence are able to compute the mass-loss rate $\dot{m}$ with Eq. (11).

We made this simplified assumption of unchanged ρ_s and r_s in order to capture the most relevant physics of tidal mass loss in our analytical modeling. According to Ref. [34], however, ρ_s and r_s do change in one orbit by $\lesssim$50%. Although we have neglected this effect in the model of tidal stripping, our results show good agreements with those of N-body simulations as we show below. This is likely due to the compensation of the changes of ρ_s and r_s with those of r_t, and therefore, our simplification does not significantly affect our estimates about the tidal mass loss of subhalos.

B. Numerical simulations

We have also calculated the tidal stripping of subhalos using N-body simulations. To cover a wide range of halo mass, we used five large cosmological N-body simulations. Table I summarizes the details of these simulations. The ν^2GC-S, ν^2GC-H2 [38], and Phi-1 simulations cover halos with a large mass ($\sim 10^{11}\ M_\odot$). The Phi-2 simulation is for intermediate mass halos ($\sim 10^7\ M_\odot$). To analyze the smallest scale ($\sim 10^{-6}\ M_\odot$), the A_N8192L800 simulation is used. The cosmological parameters of these simulations are $\Omega_m = 0.31$, $\lambda_0 = 0.69$, $h = 0.68$, $n_s = 0.96$, and $\sigma_8 = 0.83$, which are consistent with an observation of the cosmic microwave background obtained by the Planck satellite [2,39] and those adopted in the other sections of the present paper. The matter power spectrum in the A_N8192L800 simulation contained the cutoff imposed by the free motion of dark matter particles with a mass of 100 GeV [9,26]. Further details of these simulations are presented in Ref. [38] and Ishiyama *et al.* (in preparation).

All simulations were conducted by a massively parallel TreePM code, GreeM [41,42].[1] Halos and subhalos were identified by ROCKSTAR phase space halo and subhalo finder [43]. Merger trees are constructed by consistent tree codes [44]. The halo and subhalo catalogs and merger trees of the ν^2GC-S, ν^2GC-H2, and Phi-1 simulations are publicly available at http://hpc.imit.chiba-u.jp/ishiymtm/db.html.

C. Comparison

We calculate the mass-loss rate of the subhalos for various redshift z and the host mass $M_{\rm host}$ (defined as M_{200}). First, we choose the subhalo mass at accretion $m_{\rm acc}$ uniformly in a logarithmic scale between the smallest mass $10^{-6}\ M_\odot$ and the maximum mass $0.1M(z_{\rm acc})$. For each set of $m_{\rm acc}$ and $z_{\rm acc}$ (as well as z and $M_{\rm host}$), we calculate the mass-loss rate $\dot{m}$ following the prescription given in Sec. III A, by taking a Monte Carlo approach, i.e., by drawing the concentration of the host halos, subhalo concentration, circularity η, and radius of the circular orbit R_c of subhalos following the distributions of each of these parameters.

In Fig. 1, we show results of our Monte Carlo simulations. We find that for a large dynamic range of subhalo mass m (over 19 orders of magnitude as shown in the insets) down to very small masses such as $10^{-6}\ M_\odot$, a single power-law function [Eq. (1)] gives a very good fit, which confirms the *physical* origin of this relation, not just being a simple phenomenological fit.

We compare the results of the Monte Carlo calculations to those of the N-body simulations as described in Sec. III B, which is also shown in Fig. 1 for $\bar{m}/M_{\rm host} \gtrsim 10^{-5}$ ($\bar{m}$ is the orbit-averaged mass of the subhalos), resolved in the N-body simulations. At relatively small redshifts for both $M_{\rm host} = 10^{13}\ M_\odot$ and $10^7\ M_\odot$, we find very good agreement between the two prescriptions. We also check the applicability of the analytical approach by comparing the results with those of N-body simulations of small-mass hosts at higher redshift, $z = 32$, for which the η distribution at $z = 7$ of Ref. [37] was adopted. Even at the very high redshift and for the very small host mass of $M_{\rm host} = 10^{-2}\ M_\odot$, we still find reasonable agreement within differences of a factor of a few in $\dot{m}$ between results obtained by the Monte Carlo approaches and the N-body simulations. Although we cannot test the validity of our Monte Carlo approach for $\bar{m}/M_{\rm host} \ll 10^{-5}$ in comparison with the N-body simulations, these agreements that have

[1] http://hpc.imit.chiba-u.jp/ishiymtm/greem/.

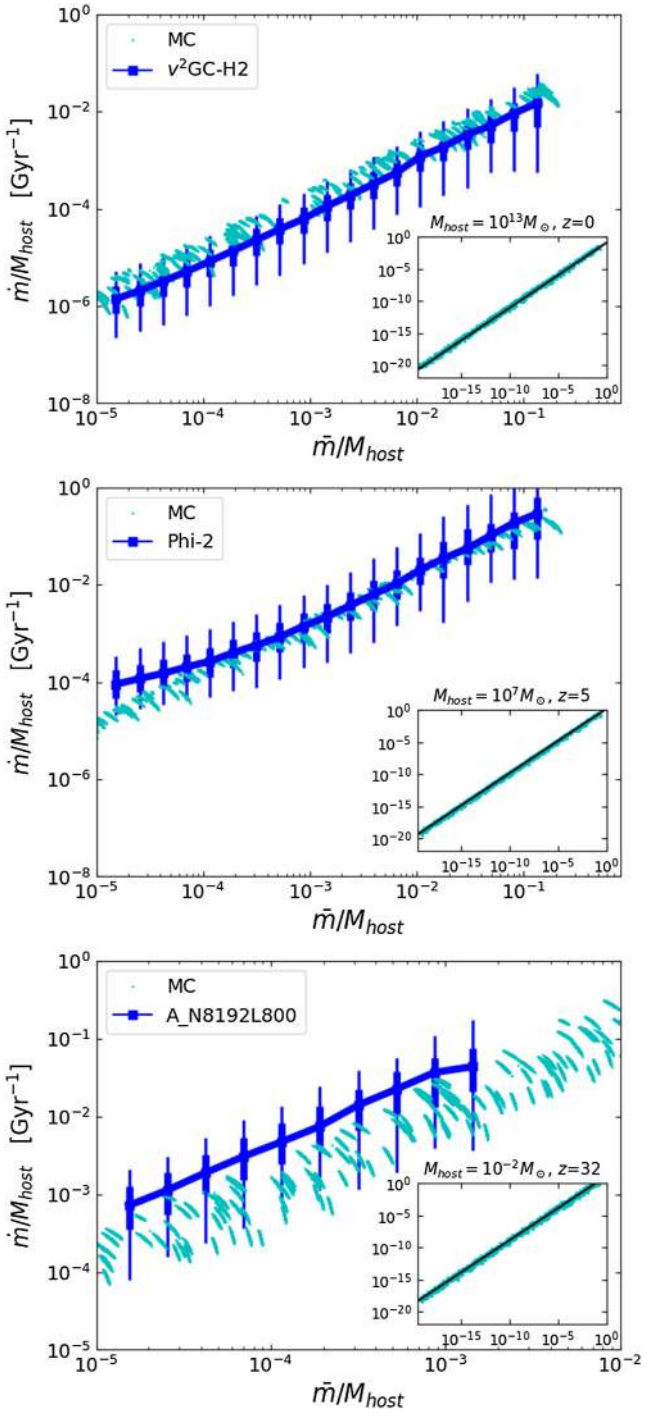

FIG. 1. Mass-loss rate of subhalos as a function of orbit-averaged subhalo mass $\bar{m}$ in units of the host mass $M_{\rm host}$ for $M_{\rm host} = 10^{13}\ M_\odot$ and $z = 0$ (top), $M_{\rm host} = 10^{7}\ M_\odot$ and $z = 5$ (middle), and $M_{\rm host} = 10^{-2}\ M_\odot$ and $z = 32$ (bottom). Cyan points show the Monte Carlo simulation results. Blue squares with error bars show the results obtained by N-body simulations. Thick error bars correspond to the 50% of the simulated halos around the median, while thin ones correspond to the 90%. We also show the results of the Monte Carlo simulations of a wider mass range in inserted panels, which also include the fitting results with Eq. (1), as overwritten solid lines on the Monte Carlo points.

been seen in Fig. 1 from very small to large hosts as well as from very high to low redshifts give us confidence that our analytical prescription captures physics of tidal stripping, and hence can be applied even to the cases with an extremely small mass ratio $\bar{m}/M_{\rm host}$.

From each calculation of $(M_{\rm host}, z)$, we fitted the values of A and ζ in Eq. (1). We then derived the dependence of A and ζ on the host mass $M_{\rm host}$ and z as

$$\log A = \left[-0.0003 \log\left(\frac{M_{\rm host}}{M_\odot}\right) + 0.02\right] z + 0.011 \log\left(\frac{M_{\rm host}}{M_\odot}\right) - 0.354, \tag{23}$$

$$\zeta = \left[0.00012 \log\left(\frac{M_{\rm host}}{M_\odot}\right) - 0.0033\right] z - 0.0011 \log\left(\frac{M_{\rm host}}{M_\odot}\right) + 0.026. \tag{24}$$

We obtain the relations, Eqs. (23) and (24), from results of the Monte Carlo simulations that cover the host mass from $M_{\rm host} = 10^{-6}\ M_\odot$ to $10^{16}\ M_\odot$ and the redshift from $z = 0$ to 7.

IV. RESULTS

By combining the tidal mass loss rate (Sec. III) with the analytical prescription for computing density profiles after tidal stripping as well as the subhalo accretion onto evolving hosts (Sec. II), we are able to calculate quantities of interest related to the subhalos. They are the subhalo mass function and the annihilation boost factor, discussed below in Secs. IV A and IV B, respectively.

We first fix the reshift of interest z_0 and the host mass at that redshift, M_0. For each set of (M_0, z_0), we uniformly sample $m_{\rm acc}$ in logarithmic space between $10^{-6}\ M_\odot$ and $0.1\ M_0$, and $z_{\rm acc}$ between $z_0 + 0.1$ and 10. Each combination is characterized by a subscript i, $(\ln m_{{\rm acc},i},\ z_{{\rm acc},i})$. Its weight w_i is chosen to be proportional to the subhalo accretion rate from the extended Press-Schechter formalism (Appendix C):

$$w_i \propto \left(\frac{d^2 N_{\rm sh}}{d \ln m_{\rm acc} dz_{\rm acc}}\right)_i. \tag{25}$$

This weight is normalized such that

$$\sum_i w_i = N_{\rm sh,total}, \tag{26}$$

where $N_{\rm sh,total}$ represents the total number of subhalos ever accreted on the given host by the time $z = z_0$. It is obtained by numerically integrating $d^2 N_{\rm sh}/(d \ln m_{\rm acc} dz_{\rm acc})$ [Eq. (C1)] over $\ln m_{\rm acc}$ and $z_{\rm acc}$. This way, we essentially approximate the integral of the distribution of $\ln m_{\rm acc}$ and $z_{\rm acc}$ as

$$\int d \ln m_{\rm acc} \int dz_{\rm acc} \frac{d^2 N_{\rm sh}}{d \ln m_{\rm acc} dz_{\rm acc}} \to \sum_i w_i. \tag{27}$$

A. Mass function of subhalos

As discussed in Sec. III A, the subhalo mass at z_0 after tidal stripping, $m_{0,i}$, is calculated by integrating Eq. (1) over cosmic time from that corresponding to $z = z_{\mathrm{acc},i}$ to $z = z_0$. The parameters A and ζ are taken from Eqs. (23) and (24), respectively. For each i, we obtain the subhalo concentrations at accretion following the log-normal distribution $P(c_{\mathrm{vir,acc}}|m_{\mathrm{acc},i}, z_{\mathrm{acc},i})$ as discussed in Sec. II and calculate the scale radius $r_{s,i}$ and characteristic density $\rho_{s,i}$ at redshift $z_{\mathrm{acc},i}$, as functions of $c_{\mathrm{vir,acc}}$. Those quantities after tidal stripping are then obtained from those before the stripping combined with the stripped mass $m_{0,i}$, as in Sec. II. If the truncation radius, $r_{t,i}$, is found smaller than $0.77 r_{s,i}$ at $z = z_0$ after the tidal stripping, we exclude the subhalo from calculation of the mass function as it is regarded as completely disrupted.

The subhalo mass function is then constructed as the distribution of $m_{0,i}$ properly weighted by w_i with the condition of tidal disruption as follows:

$$\frac{dN_{\mathrm{sh}}}{dm} = \sum_i w_i \delta(m - m_{0,i}) \times \int dc_{\mathrm{vir,acc}} P(c_{\mathrm{vir,acc}}|m_{\mathrm{acc},i}, z_{\mathrm{acc},i}) \times \Theta[r_{t,i}(z_0|c_{\mathrm{vir,acc}}) - 0.77 r_{s,i}(z_0|c_{\mathrm{vir,acc}})], \quad (28)$$

where $\delta(x)$ and $\Theta(x)$ are the Dirac delta function and Heaviside step function, respectively.

The subhalo mass function has been studied most commonly through N-body simulations in the literature. We show $m^2 dN_{\mathrm{sh}}/dm$ obtained by the numerical simulations and by our analytical model [Eq. (28)] in Fig. 2. In the top panel of Fig. 2, we compare the subhalo mass function for host masses $M_{\mathrm{host}} = 1.8 \times 10^{12}\ M_\odot$ and $5.9 \times 10^{14}\ M_\odot$ at $z = 0$ with the functions fitting to the results of Refs. [20,45], respectively. In both cases, the simulations and analytical models show reasonable agreement, while our model predicts fewer subhalos. We also show the results of ν^2GC-S, ν^2GC-H2, and Phi-1 simulations, all of which show better agreement with our analytical results. In the middle panel of Fig. 2, we compare the mass function at $z = 2$ and $z = 4$ with the results of Ref. [46] as well as ν^2GC-H2, for the host that has the mass of $M_{\mathrm{host}} = 10^{13}\ M_\odot$ at $z = 0$. This again shows very good agreement between the two approaches, where the subhalos are resolved in the numerical simulations. Our model can also be applied to cases of even smaller hosts. In the bottom panel of Fig. 2, we compare the subhalo mass function for $M_{\mathrm{host}} = 10^6\ M_\odot$ and $10^7\ M_\odot$ at $z = 5$ with the results of the Phi-2 simulations. Down to the resolution limit of the simulations that are around 500–1000 $M_\odot$, both the calculations agree well. Hence, the subhalo mass functions from our analytical model are well calibrated to the results

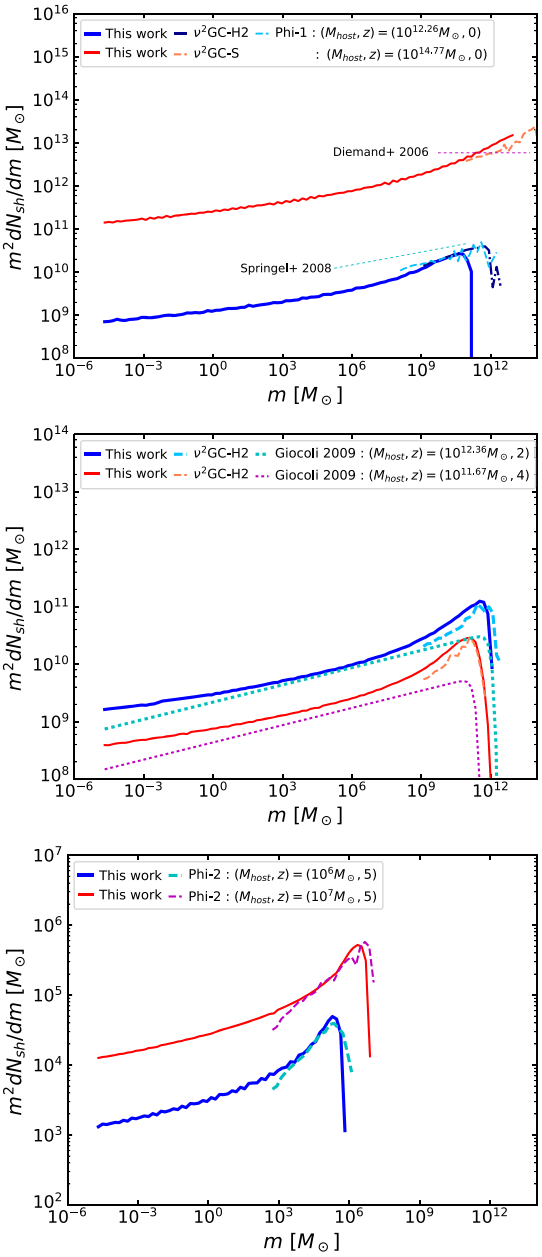

FIG. 2. Mass function of subhalos and comparison with the results of numerical simulations. Top: Comparison at $z = 0$. Thick (blue) lines correspond to the case of $M_{\mathrm{host}} = 1.8 \times 10^{12}\ M_\odot$ while thin (red) lines correspond to $5.9 \times 10^{14}\ M_\odot$. Solid lines show the mass function obtained in our analytical modelings and dashed lines show those obtained by the N-body simulations in Table I. Fitting functions in Ref. [20] for $M_{\mathrm{host}} = 1.8 \times 10^{12}\ M_\odot$ and in Ref. [45] for $5.9 \times 10^{14}\ M_\odot$ are also shown for comparison. Middle: Cases of $M_{\mathrm{host}} = 2.3 \times 10^{12}\ M_\odot$ at $z = 2$ (solid, blue line) and $M_{\mathrm{host}} = 4.7 \times 10^{11}\ M_\odot$ at $z = 4$ (thin, red line) in comparison again with the simulations in Table I and Ref. [46]. Bottom: Comparison at $z = 5$ for the cases of $M_{\mathrm{host}} = 10^6\ M_\odot$ (solid, blue lines) and $10^7\ M_\odot$ (thin, red lines) with the Phi-2 simulations. Note that some of the lines corresponding to our N-body simulations extend toward large masses, because halos of various masses around a given geometric mean have been stacked in order to derive the mass functions.

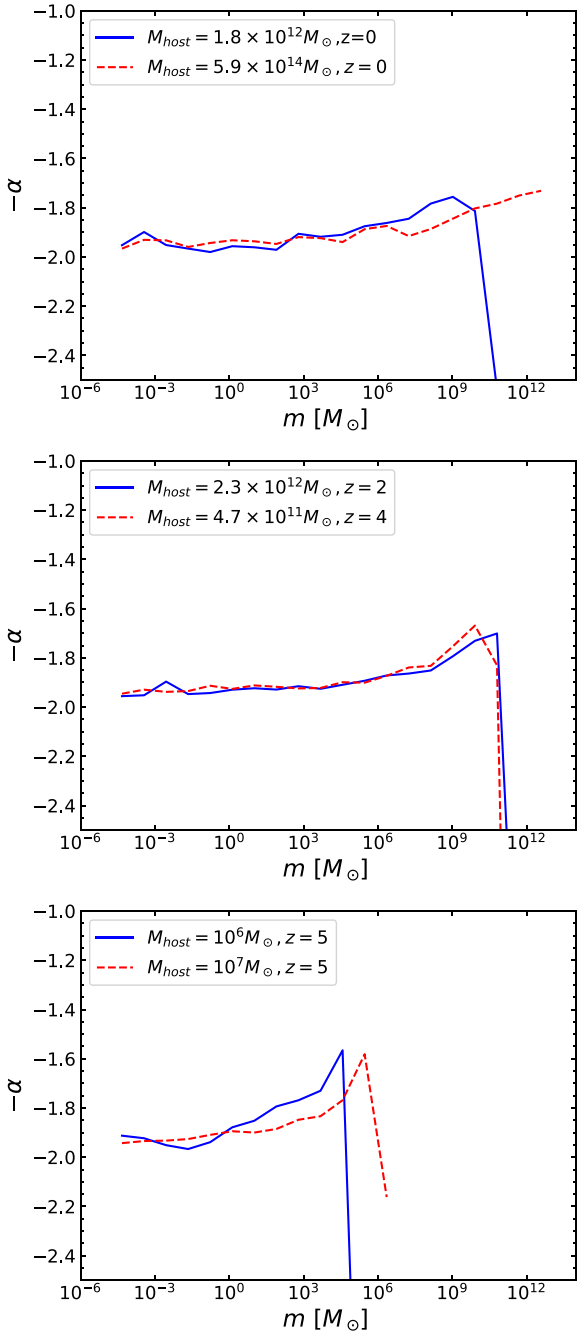

FIG. 3. The slope of the subhalo mass function $-\alpha = d\ln(dN_{\rm sh}/dm)/d\ln m$ as a function of m. The slope was averaged over mass bins of width $\Delta \log m = 1$.

of the numerical simulations at high masses, and since it is physically motivated, the behavior at the low-mass end down to very small masses can also be regarded as reliable.

In Fig. 3, we show the slope of the subhalo mass function

$$-\alpha = \frac{d\ln(dN_{\rm sh}/dm)}{d\ln m} \tag{29}$$

(i.e., $dN_{\rm sh}/dm \propto m^{-\alpha}$) for the same models as in Fig. 2. We find that the slope lies in a range between -2 and -1.8 for a large range of m except for lower and higher edges where the mass function features cutoffs. This is consistent with one of the findings from the numerical simulations, again confirming validity of our analytical model.

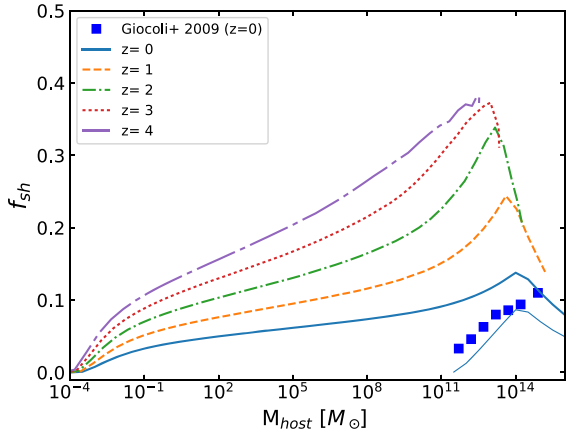

FIG. 4. Mass fraction of the host halo in the form of subhalos, $f_{\rm sh}$ as a function of $M_{\rm host}$, for $z = 0$, 1, 2, 3, and 4. Blue squares represent the subhalo mass fractions in Ref. [46], which are derived using subhalos with masses between $1.73 \times 10^{10} h^{-1}\ M_\odot$ and $0.1 M_{\rm host}$. The solid thin line shows the corresponding subhalo mass fraction in our calculation.

Figure 4 shows the mass fraction of the host mass that is contained in the form of the subhalos:

$$f_{\rm sh} = \frac{1}{M_{\rm host}} \int_{10^{-6}\ M_\odot}^{0.1 M_{\rm host}} dm m \frac{dN_{\rm sh}}{dm}. \tag{30}$$

At $z = 0$, this fraction is smaller than the $\sim$10% level up to cluster-size halos. We also find that $f_{\rm sh}$ is larger for higher redshifts, as the effect of the tidal mass loss is suppressed compared with the case of $z = 0$. In Fig. 4, we also show the results of N-body simulations by Ref. [46] for the subhalo mass fraction between $1.73 \times 10^{10} h^{-1}\ M_\odot$ and $0.1 M_{\rm host}$, which is in good agreement with our analytical result for the same quantity.

B. Subhalo boost

1. Case of smooth subhalos

The gamma-ray luminosity from dark matter annihilation in the smooth NFW component of the host halo with mass M and redshift z is obtained as

$$L_{\rm host}(M) \propto \int dc_{\rm vir} P(c_{\rm vir}|M,z) \rho_s^2 r_s^3 \left[1 - \frac{1}{(1+c_{\rm vir})^3}\right], \tag{31}$$

where $P(c_{\rm vir}|M,z)$ is again the log-normal distribution of the host's concentration parameter given M and z, and the scale radius r_s and the characteristic density ρ_s are both

dependent on $c_{\rm vir}$ as well as on M and z. The constant of proportionality of this relation includes particle physics parameters such as the mass and annihilation cross section of dark matter particles, but since here we are interested in the ratio of the luminosities between the subhalos and the host, their dependence cancels out.

Subhalo boost factor quantifies the contribution of all the subhalos to the total annihilation yields compared with the contribution from the host. It is defined as

$$B_{\rm sh}(M) = \frac{L_{\rm sh}^{\rm total}(M)}{L_{\rm host}(M)}, \tag{32}$$

such that the total luminosity from the halo is given as $L_{\rm total} = (1 + B_{\rm sh})L_{\rm host}$. The luminosity from a single subhalo i characterized with its accretion mass $m_{{\rm acc},i}$ and redshift $z_{{\rm acc},i}$, as well as its virial concentration $c_{\rm vir,acc}$, is

$$L_{{\rm sh},i} \propto \rho_{s,i}^2 r_{s,i}^3 \left[1 - \frac{1}{(1 + r_{t,i}/r_{s,i})^3}\right], \tag{33}$$

where $r_{s,i}$, $r_{t,i}$, and $\rho_{s,i}$ are the scale radius, truncation radius, and characteristic density of the subhalo i after it experienced the tidal mass loss, and hence they are functions of $m_{{\rm acc},i}$, $z_{{\rm acc},i}$, and $c_{\rm vir,acc}$ as well as the mass of the host M and redshift z (Sec. II). The total subhalo luminosity $L_{\rm sh}^{\rm total}(M)$ is then obtained as the sum of $L_{{\rm sh},i}$ with weight w_i and averaged over $c_{\rm vir,acc}$ with its distribution:

$$\begin{aligned} L_{\rm sh}^{\rm total}(M) = \sum_i w_i \int dc_{\rm vir,acc} P(c_{\rm vir,acc}|m_{{\rm acc},i}, z_{{\rm acc},i}) \\ \times L_{{\rm sh},i}(z|c_{\rm vir,acc}) \\ \times \Theta[r_{t,i}(z|c_{\rm vir,acc}) - 0.77 r_{s,i}(z|c_{\rm vir,acc})]. \end{aligned} \tag{34}$$

2. Presence of sub-subhalos

The discussions above, especially Eq. (33), are based on the assumption that the density profile of subhalos is given by a smooth NFW function. Subhalos, however, contain their own subhalos: i.e., sub-subhalos, which again contain sub-sub-subhalos, and so on. This is because the subhalos, before accreting onto their host, were formed by mergers and accretion of even smaller halos. In the following, we refer to them as sub^n-subhalos; the discussion above corresponds to the case of $n = 0$, where subhalos do not include sub-subhalos.

We include the effect of sub^n-subhalos iteratively. In the case of $n \geq 1$, when a subhalo i accretes at $z_{{\rm acc},i}$ with a mass $m_{{\rm acc},i}$, we give it a sub-subhalo boost $B_{\rm sh}^{(n-1)}(m_{{\rm acc},i}, z_{{\rm acc},i})$ obtained from the previous iteration; for $n = 1$, it is Eq. (32) evaluated at $m_{{\rm acc},i}$ and $z_{{\rm acc},i}$. After the subhalo experience the mass loss, its sub-subhalos as well as the smooth component are stripped away up to the tidal radius $r_{t,i}$. Since the sub-subhalo distribution (that the gamma-ray brightness profile from the sub-subhalos follows) is flatter than the brightness profile of the subhalo's smooth component that is proportional to the NFW profile squared, the sub-subhalo boost decreases. In order to quantify this effect, we assume that the sub-subhalos are distributed as $n_{\rm ssh}(r) \propto (r^2 + r_s^2)^{-3/2}$ (see, e.g., Ref. [47] and references therein), and further assuming that r_s and ρ_s hardly change after mass loss, the total sub-subhalo luminosity enclosed within r is

$$L_{{\rm ssh},i}(< r) \propto \ln\left[\sqrt{1 + \left(\frac{r}{r_{s,i}}\right)^2} + \frac{r}{r_{s,i}}\right] - \frac{r}{\sqrt{r^2 + r_{s,i}^2}}. \tag{35}$$

On the other hand, the enclosed luminosity from the smooth NFW component is

$$L_{{\rm sh},i}(< r) \propto 1 - \left(1 + \frac{r}{r_{s,i}}\right)^{-3}. \tag{36}$$

The sub-subhalo boost for the subhalo i at redshift z after the nth iteration is therefore estimated as

$$\begin{aligned} B_{{\rm ssh},i}^{(n)}(z) = B_{\rm sh}^{(n-1)}(m_{{\rm acc},i}, z_{{\rm acc},i}) \\ \times \frac{L_{{\rm ssh},i}(< r_{t,i})/L_{{\rm ssh},i}(< r_{{\rm vir},i})}{L_{{\rm sh},i}(< r_{t,i})/L_{{\rm sh},i}(< r_{{\rm vir},i})}, \end{aligned} \tag{37}$$

where $r_{{\rm vir},i}$ is the virial radius of the subhalo i at accretion.

We finally obtain the subhalo boost factor after the nth iteration (that takes up to sub^{n-1}-subhalos into account), $B_{\rm sh}^{(n)}(M, z)$, by combining Eqs. (31)–(34), but also by multiplying $L_{{\rm sh},i}$ in Eq. (33) with $1 + B_{{\rm ssh},i}^{(n)}(z_0)$ [Eq. (37)]. In this calculation, we consider the subhalos accreted after $z = 10$, which assures that we can follow the mass loss of the subhalos contributing to the boost factor at $z < 5$. Figure 5 shows the boost factor $B_{\rm sh}$ as a function of host mass $M_{\rm host}$ (defined as M_{200}) for several redshifts, after the fourth iteration that takes up to sub^3-subhalos into account. For $z = 0$, the subhalo boost increases gradually with the mass of the hosts and reaches to about a factor of 10 for cluster-size halos. The boost for high redshifts is still significant, being on the order of one, for a wide range of host masses.

In Fig. 6, we investigate the effect of higher-order substructure: sub^n-subhalos. Including no sub-substructure ($n = 0$) would underestimate the boost by about a factor of a few for massive host halos such as galaxies and clusters. We find that the boost saturates after the third iteration, after which further enhancement is of the several percent level.

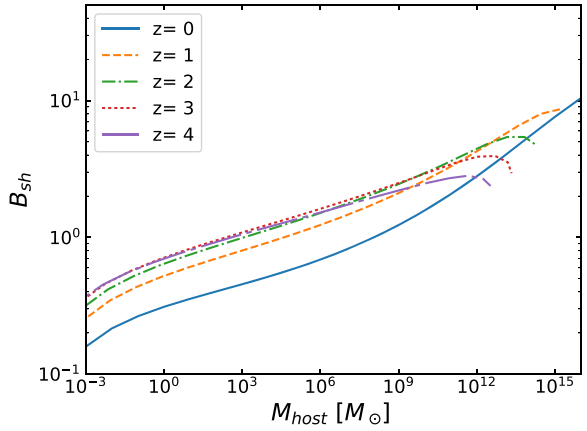

FIG. 5. Boost factor $B_{\rm sh} = L_{\rm sh}^{\rm total}/L_{\rm host}$ as a function of the host mass $M_{\rm host}$ (defined as M_{200}) between 10^{-3} $M_\odot$ and 10^{16} $M_\odot$ at observation redshifts $z = 0$, 1, 2, 3, and 4. The calculations include up to sub^3-subhalos.

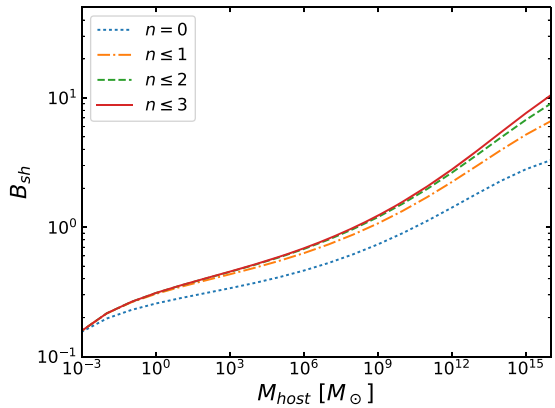

FIG. 6. Subhalo boost factor at $z = 0$ including sub^n-subhalos; i.e., the nth sub-substructure.

V. DISCUSSION

A. Comparison with earlier work

The current work updated an analytical model of Ref. [27], by (i) implementing the scatter distribution in the concentration-mass relation for both the host and subhalos, (ii) calibrating the subhalo mass-loss rate down to extremely small mass ratio m/M using the Monte Carlo simulations of the tidal stripping, (iii) extending the calculations of the boost factor as well as the subhalo mass function beyond $z = 0$, and (iv) including sub-subhalos and beyond. They are all essential ingredients to improve the accuracy of the subhalo modeling, and hence the current work is regarded as a direct update of Ref. [27]. As the quantitative outcome, we find that the subhalo boost without a contribution from sub-subhalos ($n = 0$) is consistent with the result of Ref. [27]. Our result including up to sub^3-subhalos further enhances the boost by a factor of 2–3 for large halos, and extends the calculation down to 10^{-4} $M_\odot$.

The effect of tidal stripping on the annihilation boost has also been studied in Refs. [48,49] by using different approaches, but they both have reached a similar conclusion to that of Ref. [27]. In particular, Ref. [49] relied directly on N-body simulations to claim that subhalos are more concentrated than field halos of equal mass, and hence, the annihilation boost is larger than previous estimates by, e.g., Ref. [50]. One of the great advantages of directly using the results from N-body simulations is its accuracy when the discussion concerns the *resolved* regime. However, each simulation is computationally demanding, and thus, it is not easy to generalize the discussion to wider ranges of host masses and redshifts. In fact, in order to compute the subhalo boost factor as a function of the host mass, Ref. [49] had to combine the subhalo concentration-mass relation with the subhalo mass function, for the latter of which a few phonomenological fitting functions calibrated with other simulations were adopted. Hence, the boost factor as its outcome shows a very large range of uncertainties depending on what model of the mass function one adopts. In our analytical approach, on the other hand, we are able to perform physics-based computations of the subhalo boost factor and mass function in a self-consistent manner, for very wide ranges of masses and redshifts.

References [51,52] developed an analytical model assuming self-similarity of the substructures, computed the probability distribution function of the dark matter density that has a power-law tail, and calibrated it with numerical simulations of the Galactic halo. The annihilation boost factor within the volume of the virial radius of ~200 kpc was found to be ~10, which is slightly larger than our result. This, however, agrees with our result based on a different model of the concentration-mass relation (see Sec. V C).

Reference [53] modeled dark matter subhalos in a Milky Way–like halo at $z = 0$ by including the effect of the disk shocking as well as the tidal stripping. Our result of the annihilation boost factor is consistent with that of Ref. [53] after integrating over the entire volume of the halo and assuming the subhalo mass function of $\propto m^{-1.9}$. Our discussion in Sec. III can be expanded to accommodate the spatial distribution of subhalos, but doing so and comparing the result with that of Ref. [53] would include proper modeling of the baryonic component, which is beyond the scope of the present work.

B. A case without tidal disruption

Reference [21] recently pointed out that the tidal disruption for the subhalos with $r_t < 0.77 r_s$ might be a numerical artifact, and many more subhalos even with much smaller truncation radius r_t could survive against the tidal disruption. In this paper, we do not argue for or against

the claim of Ref. [21], but simply study the implication of the claim as an optimistic example. To this end, we repeated the boost calculations without implementing the constraint $r_t > 0.77 r_s$; i.e., all the subhalos survive no matter how much mass they lose due to the tidal stripping. We find that the obtained boost factor hardly changes at any redshift.

C. Dependence on the concentration-mass relation

In our calculations of the boost factor, we adopted the mass-concentration relation in Ref. [31] as the canonical model. Their derivation is based on the analysis with N-body simulations. Reference [54] proposed a different concentration-mass relation based on analytical considerations, which expect higher concentration especially around $z = 0$. In order to compare the dependence of the boost factor on the different concentration-mass relations, we also calculated the boost factor adopting the relation in Ref. [54]. In Fig. 7, we show that the boost factor enhances by more than a factor of a few if we adopt the concentration-mass relation of Ref. [54] instead of that of Ref. [31]. The obtained boost factor directly reflects the difference of the concentrations at around $z = 0$. We do not discuss the feasibility of these concentrations since that is beyond the scope of this paper. Our results show that a deeper understanding of the concentration-mass relation is necessary to obtain the boost factor corresponding to the actual situations.

In Ref. [55], there are some discussions about the mass-concentration relation and the primordial curvature perturbations in the early Universe. If the primordial power spectrum has a feature that gives rise to ultracompact minihalos, it may boost dark matter annihilation even more significantly by changing density profiles and the concentration-mass relation. Although evaluating the subhalo boost for these specific models is beyond the scope of our work, we note that such a significant boost predicted by Refs. [55,56] may already be constrained very strongly using the existing gamma-ray data.

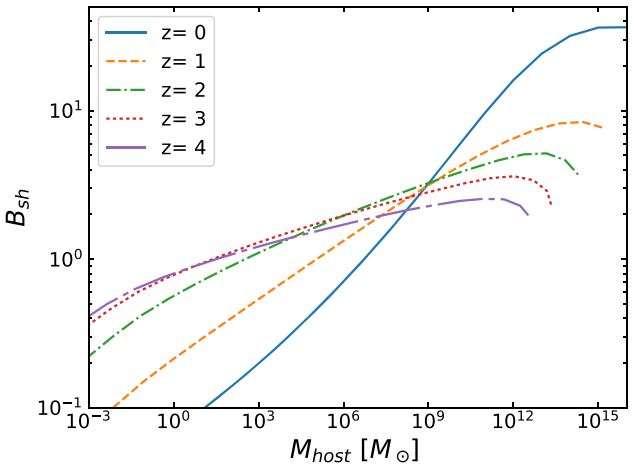

FIG. 7. The same as Fig. 5, but for the concentration-mass relation in Ref. [54].

D. Contribution to the isotropic gamma-ray background

One of the advantages of our analytical model of the subhalo boost is the capability of calculating the isotropic gamma-ray background (IGRB) from dark matter annihilation, since we can compute boost factors for various host masses and the wide range of redshifts, self-consistently. The intensity of IGRB was most recently measured with Fermi-LAT [57], which was then used to constrain the dark matter annihilation cross section (e.g., [58]).

We followed the "halo model" approach of Ref. [47] to compute the IGRB contribution from dark matter annihilation, but by applying the results of the annihilation boost factor from our analytical model (Fig. 5) as well as by including scatter of the concentration-mass relation. Figure 8 shows the IGRB intensity from dark matter annihilation in the case of the canonical annihilation cross section for the thermal freeze-out scenario, $\langle \sigma v \rangle \simeq 2 \times 10^{-26}$ cm^3 s^{-1} [59], dark matter mass of $m_\chi = 100$ GeV, and $b\bar{b}$ final state of the annihilation ($\chi\chi \to b\bar{b}$). Our boost model enhances the IGRB intensity by a factor of a few compared with the case of no subhalo boost. Note that a contribution from the Galactic subhalos (e.g., [60]) is not included, and hence our estimate is conservative.

We then performed a simple analysis of the Fermi-LAT IGRB data [58]. We included two components: (1) dark matter annihilation of a given mass m_χ and assuming $b\bar{b}$ final states, and (2) an "astrophysical" power-law component with a cutoff, for which we adopt the best-fit

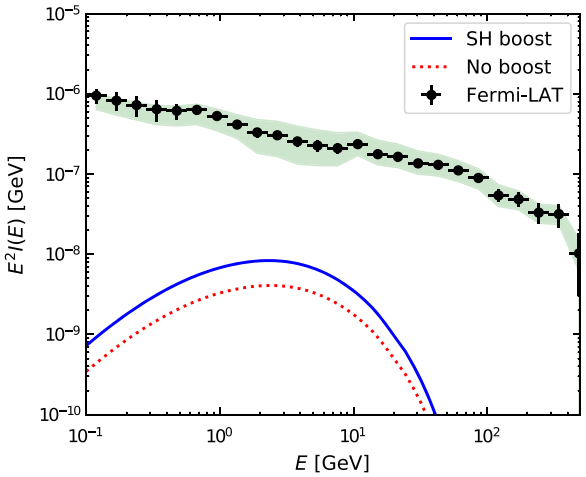

FIG. 8. Contribution to the IGRB intensity measured by Fermi-LAT from dark matter annihilation for $\langle \sigma v \rangle = 2.2 \times 10^{-26}$ cm^3 s^{-1}, $m_\chi = 100$ GeV, and $b\bar{b}$ final state. The solid (dotted) curve shows the case of the subhalo boost (no boost).

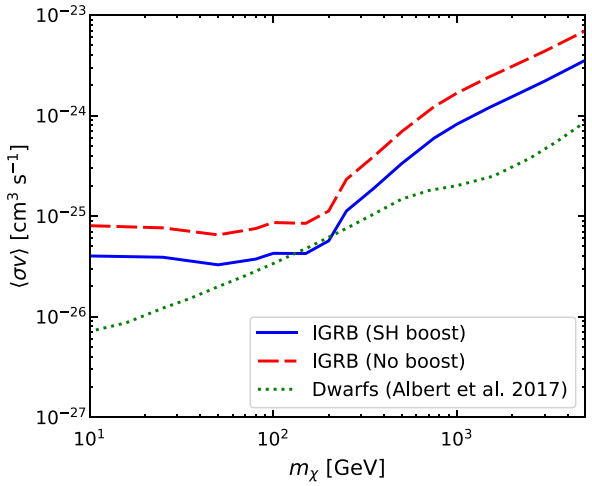

FIG. 9. Upper limits on the dark matter annihilation cross section at 95% confidence level as a function of dark matter mass for $b\bar{b}$ final state. Solid and dashed curves are for the canonical boost model and without the subhalo boost, respectively. For comparison, the results of the latest joint-likelihood analysis of 41 dwarfs [63] are shown as a dotted curve.

spectral shape, $I_{\rm astro}(E) \propto E^{-2.32}\exp(-E/279\ {\rm GeV})$ [58]. By adopting normalizations of these components as two free parameters for the fit, we performed a χ^2 analysis in order to obtain the upper limits on $\langle\sigma v\rangle$. For the IGRB data, we adopt those for a foreground model "A" in Ref. [58], but treat statistical and systematic uncertainties as independent errors. Figure 9 shows the upper limits on $\langle\sigma v\rangle$ at 95% confidence level ($\Delta\chi^2 = 2.71$) using our canonical boost model as well as the case of no boost. Our updated boost model improves the limits by a factor of a few nearly independently of dark matter mass (see also, e.g., Refs. [61,62] for earlier results). This enhancement is calculated consistently as our formalism automatically computes all the subhalo properties at once including the mass function and the boost factor. We also compare our limits with the latest results of the joint likelihood analysis of 41 dwarf spheroidal galaxies [63], which set the benchmark as the most robust constraints on dark matter annihilation.

Although some improvements of the limit obtained from the observations of dwarf spheroidal galaxies also can be expected, we conservatively neglect this contribution according to the discussion in Ref. [27]. We find that the IGRB limits with our boost model are competitive to the dwarf bounds for dark matter masses at ∼200 GeV. Note that more accurate limits should include uncertainties coming from modeling of the astrophysical contributions. Further consideration is needed in order to obtain correct values, which is slated for future works. (See also Ref. [64] for a detailed discussion on various sources of uncertainties.)

The small-scale angular power spectrum of the IGRB has also been measured with Fermi-LAT [65], which provides yet another avenue to constrain dark matter annihilation [47,66] as well as high-energy astrophysical sources [67,68]. It is also pointed out that taking cross-correlations with local gravitational tracers such as galaxy catalogs is a promising way along the same line [69–71]. Since these *anisotropy* constraints are more sensitive to the dark matter distribution at smaller redshifts and in larger hosts, the effect of the subhalo boost is expected to be even more important than for the IGRB intensity. A dedicated investigation is beyond the scope of this work and hence is reserved as a subject for a future paper. We also note that our updated boost model will impact the result of the stacking analysis of nearby galaxy groups [72], which relied on the boost model of Ref. [27].

VI. CONCLUSIONS

We can access the substructure of dark matter halos which is beyond the resolutions of the numerical simulations by taking an analytical approach on the modeling of the tidal mass loss of the subhalos. We analytically modeled the mass loss of subhalos under the gravitational potential of their hosts, following the evolution of both the host and the subhalos in a self-consistent way. In order to take distributions of the concentrations of the hosts, orbits, and concentrations of subhalos into account, we conducted Monte Carlo simulations. We find that the mass loss of the subhalos is well described with Eq. (1) down to the scale of $m/M_{\rm host} \sim \mathcal{O}(10^{-19})$, and it agrees well with the results of N-body simulations.

Combining the derived relation about the subhalo mass loss with analytical models for mass and redshift distributions of accreting subhalos, we calculated the subhalo mass functions and the boost factor for dark matter annihilation. We showed that mass functions of subhalos derived in our analytical modeling are consistent with those obtained in N-body simulations down to their resolution limits. From our model of the subhalo boost of dark matter annihilation, we expect enhancement in the gamma-ray signals by up to a factor of ∼10 because of the remaining substructures in larger halos, predicting promising opportunities for detecting particle dark matter in future gamma-ray observations. Including substructures in the subhalos will give an important contribution to the annihilation boost up to a factor of a few.

The results of our calculations are consistent with both earlier analytical and numerical approaches, but are applicable to much wider (and arbitrary) range of host masses and redshifts, and hence can be used to predict gamma-ray flux from dark matter annihilation in various halos at any redshifts. As an example, we computed the contribution to the isotropic gamma-ray background from our boost model. We find that the presence of subhalos (and their substructures) enhance the gamma-ray intensity by a factor of a few, and hence the limits on the annihilation cross section improves by the same factor, excluding the region of $\langle\sigma v\rangle \gtrsim 4\times10^{-26}$ cm^3 s^{-1} for dark matter masses smaller than ∼200 GeV.

ACKNOWLEDGMENTS

We thank Richard Bartels for discussions. This work was supported by JSPS KAKENHI Grants No. 17H04836 (S. A.), No. 15H01030 and No. 17H04828 (T. I.). Numerical computations were partially carried out on the K computer at the RIKEN Advanced Institute for Computational Science (Proposals No. hp150226, No. hp160212, No. hp170231), and Aterui supercomputer at Center for Computational Astrophysics, CfCA, of National Astronomical Observatory of Japan. T. I. has been supported by MEXT as "Priority Issue on Post-K computer" (Elucidation of the Fundamental Laws and Evolution of the Universe) and Joint Institute for Computational Fundamental Science (JICFuS).

APPENDIX A: MASS EVOLUTION OF HOST HALOS

In order to calculate the evolution of subhalos, we first specify how the hosts that are not in an even larger halo evolve. The authors of Ref. [28] derive the relations about the mass accretion history of the halos $M(z|M_0, z=0)$, i.e., the mass of the halo at redshift z, whose mass is M_0 at $z=0$,

$$M(z|M_0, z=0) = M_0(1+z)^{\alpha}\exp(\beta z), \tag{A1}$$

with

$$\beta = -g(M_0), \tag{A2}$$

$$\alpha = \left[\frac{1.686\sqrt{2/\pi}}{D^2(z=0)}\frac{dD}{dz}\bigg|_{z=0} + 1\right] g(M_0), \tag{A3}$$

$$g(M_0) = [S(M_0/q) - S(M_0)]^{-1/2}, \tag{A4}$$

$$q = 4.137\tilde{z}_f^{-0.9476}, \tag{A5}$$

$$\tilde{z}_f = -0.0064(\log M_0)^2 + 0.0237(\log M_0) + 1.8837, \tag{A6}$$

where $D(z)$ and $S(M) \equiv \sigma^2(M)$ are the growth function and the variance of the matter distribution at mass scale M and $z=0$, respectively. We adopt fitting functions of both $D(z)$ and $\sigma(M)$ from Ref. [73]. Equation (A1) is generalized to determine the mass of halos $M(z|M(z_i), z_i)$ at redshift z, whose mass was $M(z_i)$ at redshift z_i [31],

$$M(z|M(z_i), z_i) = M(z_i)(1+z-z_i)^{\alpha}\exp(\beta(z-z_i)), \tag{A7}$$

with replacing M_0 with $M(z_i)$ in Eqs. (A2), (A3), and (A4). These relations enable us to follow back the evolutions of the hosts starting from any redshift adopting the generalized equations.

APPENDIX B: CONCENTRATION-MASS RELATION OF THE FIELD HALOS

We here summarize the concentration-mass relation $c_{200}(M_{200})$ for the field halos based on Ref. [31], which is adopted throughout this paper. We take the fitted values corresponding to the Planck cosomlogy.

For $z \le 4$

$$\log c_{200} = \alpha + \beta\log\left(\frac{M_{200}}{M_\odot}\right)\left[1 + \gamma\log^2\left(\frac{M_{200}}{M_\odot}\right)\right], \tag{B1}$$

where

$$\alpha = 1.7543 - 0.2766(1+z) + 0.02039(1+z)^2, \tag{B2}$$

$$\beta = 0.2753 + 0.00351(1+z) - 0.3038(1+z)^{0.0269}, \tag{B3}$$

$$\gamma = -0.01537 + 0.02102(1+z)^{-0.1475}, \tag{B4}$$

and for $z > 4$,

$$\log c_{200} = \alpha + \beta\log\left(\frac{M_{200}}{M_\odot}\right), \tag{B5}$$

where

$$\alpha = 1.3081 - 0.1078(1+z) + 0.00398(1+z)^2, \tag{B6}$$

$$\beta = 0.0223 - 0.0944(1+z)^{-0.3907}. \tag{B7}$$

APPENDIX C: SUBHALO ACCRETION RATE

With the understanding of the growth history of certain hosts, we know the distributions of the mass and redshift of the accreting subhalos on that host. The authors of Ref. [36] studied the mass accretion history and obtained the distribution $d^2N_{\rm sh}/(d\ln m_{\rm acc} dz_{\rm acc})$: the number of subhalos accreted onto the host per unit logarithmic mass range around $\ln m_{\rm acc}$ and per unit redshift range around accretion redshift $z_{\rm acc}$,

$$\frac{d^2N_{sh}}{d\ln m_{\rm acc} dz_{\rm acc}} = \mathcal{F}(s_{\rm acc}, \delta_{\rm acc}|S_0, \delta_0; \bar{M}_{\rm acc})\frac{ds_{\rm acc}}{dm_{\rm acc}}\frac{d\bar{M}_{\rm acc}}{dz_{\rm acc}}, \tag{C1}$$

where following the convention of Ref. [36], $s_{\rm acc}$ and $\delta_{\rm acc}$ are used to parametrize the mass and redshift, respectively, since they are defined as $s_{\rm acc} \equiv \sigma^2(m_{\rm acc}, z=0)$ and $\delta_{\rm acc} = \delta_c(z_{\rm acc}) = 1.686/D(z_{\rm acc})$ [73]. Similarly, for the host, we adopt $S_0 = \sigma^2(M_0, z=0)$ and $\delta_0 = \delta_{\rm sc}(z_0)$ to characterize the mass M_0 and redshift z_0 as a boundary condition. The mass of the host $M_{\rm acc}$ at the accretion redshift $z_{\rm acc}$ (that eventually evolves to M_0 at z_0) follows the probability distribution $P(M_{\rm acc}|S_0, \delta_0)$, for which we adopt a log-normal distribution with a logarithmic mean $\bar{M}_{\rm acc} = M(z_{\rm acc}|M_0, z_0)$ [Eq. (A7)] and a logarithmic dispersion

$$\sigma_{\log M_{\rm acc}} = 0.12 - 0.15\log\left(\frac{M_{\rm acc}}{M_0}\right). \tag{C2}$$

The definition of the function $\mathcal{F}$ in Eq. (C1) is

$$\mathcal{F}(s_{\rm acc},\delta_{\rm acc}|S_0,\delta_0;\bar{M}_{\rm acc}) = \int \Phi(s_{\rm acc}.\delta_{\rm acc}|S_0,\delta_0;M_{\rm acc})P(M_{\rm acc}|S_0,\delta_0)dM_{\rm acc}, \tag{C3}$$

$$\Phi(s_{\rm acc},\delta_{\rm acc}|S_0,\delta_0;M_{\rm acc}) = \left[\int_{S(m_{\rm max})}^{\infty} F(s_{\rm acc},\delta_{\rm acc}|S_0,\delta_0;M_{\rm acc})ds_{\rm acc}\right]^{-1} \times \begin{cases} F(s_{\rm acc},\delta_{\rm acc}|S_0,\delta_0;M_{\rm acc}), & (m_{\rm acc}\le m_{\rm max}), \\ 0, & (\text{otherwise}), \end{cases} \tag{C4}$$

$$F(s_{\rm acc},\delta_{\rm acc}|S_0,\delta_0;M_{\rm acc}) = \frac{1}{\sqrt{2\pi}}\frac{\delta_{\rm acc}-\delta_M}{(s_{\rm acc}-S_M)^{3/2}}\exp\left[-\frac{(\delta_{\rm acc}-\delta_M)^2}{2(s_{\rm acc}-S_M)}\right], \tag{C5}$$

where $m_{\rm max}=\min[M_{\rm acc},M_0/2]$ and $M_{\rm max}=\min[M_{\rm acc}+m_{\rm max},M_0]$ are introduced such that the mass hierarchy of the host mass before and after subhalo accretions is assured, $S_M=\sigma_M^2(M_{\rm max})$ and δ_M is defined as $\delta_{\rm sc}(z)$ at a redshift at which $M=M_{\rm max}$. The equations above determine the distributions of accreting subhalos $d^2N_{\rm sh}/(d\ln m_{\rm acc}dz_{\rm acc})$ for arbitrary hosts.

[1] P. J. E. Peebles, Large scale background temperature and mass fluctuations due to scale invariant primeval perturbations, Astrophys. J. **263**, L1 (1982).
[2] P. A. R. Ade *et al.* (Planck Collaboration), Planck 2015 results. XIII. Cosmological parameters, Astron. Astrophys. **594**, A13 (2016).
[3] T. S. van Albada, J. N. Bahcall, K. Begeman, and R. Sancisi, The distribution of dark matter in the spiral galaxy NGC-3198, Astrophys. J. **295**, 305 (1985).
[4] P. Salucci and A. Borriello, The intriguing distribution of dark matter in galaxies, Lect. Notes Phys. **616**, 66 (2003).
[5] D. Clowe, A. Gonzalez, and M. Markevitch, Weak lensing mass reconstruction of the interacting cluster 1E0657-558: Direct evidence for the existence of dark matter, Astrophys. J. **604**, 596 (2004).
[6] G. Jungman, M. Kamionkowski, and K. Griest, Supersymmetric dark matter, Phys. Rep. **267**, 195 (1996).
[7] J. M. Gaskins, A review of indirect searches for particle dark matter, Contemp. Phys. **57**, 496 (2016).
[8] S. Hofmann, D. J. Schwarz, and H. Stoecker, Damping scales of neutralino cold dark matter, Phys. Rev. D **64**, 083507 (2001).
[9] A. M. Green, S. Hofmann, and D. J. Schwarz, The power spectrum of SUSY-CDM on sub-galactic scales, Mon. Not. R. Astron. Soc. **353**, L23 (2004).
[10] S. Profumo, K. Sigurdson, and M. Kamionkowski, What Mass Are the Smallest Protohalos?, Phys. Rev. Lett. **97**, 031301 (2006).
[11] R. Diamanti, M. E. C. Catalan, and S. Ando, Dark matter protohalos in a nine parameter MSSM and implications for direct and indirect detection, Phys. Rev. D **92**, 065029 (2015).
[12] F. C. van den Bosch, G. Tormen, and C. Giocoli, The mass function and average mass loss rate of dark matter subhaloes, Mon. Not. R. Astron. Soc. **359**, 1029 (2005).
[13] C. Giocoli, L. Pieri, and G. Tormen, Analytical approach to subhaloes population in dark matter haloes, Mon. Not. R. Astron. Soc. **387**, 689 (2008).
[14] F. Jiang and F. C. van den Bosch, Statistics of dark matter substructure. I. Model and universal fitting functions, Mon. Not. R. Astron. Soc. **458**, 2848 (2016).
[15] J. Penarrubia and A. J. Benson, Effects of dynamical evolution on the distribution of substructures, Mon. Not. R. Astron. Soc. **364**, 977 (2005).
[16] L. Gao, S. D. M. White, A. Jenkins, F. Stoehr, and V. Springel, The subhalo populations of lambda-CDM dark halos, Mon. Not. R. Astron. Soc. **355**, 819 (2004).
[17] J. Diemand, M. Kuhlen, and P. Madau, Formation and evolution of galaxy dark matter halos and their substructure, Astrophys. J. **667**, 859 (2007).
[18] C. Giocoli, G. Tormen, and F. C. v. d. Bosch, The population of dark matter subhaloes: Mass functions and average mass loss rates, Mon. Not. R. Astron. Soc. **386**, 2135 (2008).
[19] K. Dolag, S. Borgani, G. Murante, and V. Springel, Substructures in hydrodynamical cluster simulations, Mon. Not. R. Astron. Soc. **399**, 497 (2009).
[20] V. Springel, J. Wang, M. Vogelsberger, A. Ludlow, A. Jenkins, A. Helmi, J. F. Navarro, C. S. Frenk, and S. D. M. White, The aquarius project: The subhalos of galactic halos, Mon. Not. R. Astron. Soc. **391**, 1685 (2008).
[21] F. C. van den Bosch, G. Ogiya, O. Hahn, and A. Burkert, Disruption of dark matter substructure: Fact or fiction?, Mon. Not. R. Astron. Soc. **474**, 3043 (2018).
[22] J. Diemand, M. Kuhlen, and P. Madau, Dark matter substructure and gamma-ray annihilation in the Milky Way halo, Astrophys. J. **657**, 262 (2007).
[23] L. E. Strigari, S. M. Koushiappas, J. S. Bullock, and M. Kaplinghat, Precise constraints on the dark matter content of Milky Way dwarf galaxies for gamma-ray experiments, Phys. Rev. D **75**, 083526 (2007).
[24] L. Pieri, G. Bertone, and E. Branchini, Dark matter annihilation in substructures revised, Mon. Not. R. Astron. Soc. **384**, 1627 (2008).
[25] T. E. Jeltema and S. Profumo, Searching for dark matter with x-ray observations of local dwarf galaxies, Astrophys. J. **686**, 1045 (2008).
[26] T. Ishiyama, Hierarchical formation of dark matter halos and the free streaming scale, Astrophys. J. **788**, 27 (2014).
[27] R. Bartels and S. Ando, Boosting the annihilation boost: Tidal effects on dark matter subhalos and consistent luminosity modeling, Phys. Rev. D **92**, 123508 (2015).

[28] C. A. Correa, J. S. B. Wyithe, J. Schaye, and A. R. Duffy, The accretion history of dark matter haloes. I. The physical origin of the universal function, Mon. Not. R. Astron. Soc. **450**, 1514 (2015).
[29] J. F. Navarro, C. S. Frenk, and S. D. M. White, A universal density profile from hierarchical clustering, Astrophys. J. **490**, 493 (1997).
[30] G. L. Bryan and M. L. Norman, Statistical properties of x-ray clusters: Analytic and numerical comparisons, Astrophys. J. **495**, 80 (1998).
[31] C. A. Correa, J. S. B. Wyithe, J. Schaye, and A. R. Duffy, The accretion history of dark matter haloes. III. A physical model for the concentration-mass relation, Mon. Not. R. Astron. Soc. **452**, 1217 (2015).
[32] W. Hu and A. V. Kravtsov, Sample variance considerations for cluster surveys, Astrophys. J. **584**, 702 (2003).
[33] T. Ishiyama, J. Makino, S. Portegies Zwart, D. Groen, K. Nitadori, S. Rieder, C. de Laat, S. McMillan, K. Hiraki, and S. Harfst, The cosmogrid simulation: Statistical properties of small dark matter halos, Astrophys. J. **767**, 146 (2013).
[34] J. Penarrubia, A. J. Benson, M. G. Walker, G. Gilmore, A. McConnachie, and L. Mayer, The impact of dark matter cusps and cores on the satellite galaxy population around spiral galaxies, Mon. Not. R. Astron. Soc. **406**, 1290 (2010).
[35] E. Hayashi, J. F. Navarro, J. E. Taylor, J. Stadel, and T. R. Quinn, The structural evolution of substructure, Astrophys. J. **584**, 541 (2003).
[36] X. Yang, H. J. Mo, Y. Zhang, and F. C. v. d. Bosch, An analytical model for the accretion of dark matter subhalos, Astrophys. J. **741**, 13 (2011).
[37] A. R. Wetzel, On the orbits of infalling satellite halos, Mon. Not. R. Astron. Soc. **412**, 49 (2011).
[38] T. Ishiyama, M. Enoki, M. A. R. Kobayashi, R. Makiya, M. Nagashima, and T. Oogi, The ν^2GC simulations: Quantifying the dark side of the universe in the Planck cosmology, Publ. Astron. Soc. Jpn. **67**, 61 (2015).
[39] P. A. R. Ade *et al.* (Planck Collaboration), Planck 2013 results. XVI. Cosmological parameters, Astron. Astrophys. **571**, A16 (2014).
[40] R. Makiya, M. Enoki, T. Ishiyama, M. A. R. Kobayashi, M. Nagashima, T. Okamoto, K. Okoshi, T. Oogi, and H. Shirakata, The new numerical galaxy catalog (ν^2GC): An updated semi-analytic model of galaxy and active galactic nucleus formation with large cosmological N-body simulations, Publ. Astron. Soc. Jpn. **68**, 25 (2016).
[41] T. Ishiyama, T. Fukushige, and J. Makino, GreeM: Massively parallel TreePM code for large cosmological N-body simulations, Publ. Astron. Soc. Jpn. **61**, 1319 (2009).
[42] T. Ishiyama, K. Nitadori, and J. Makino, 4.45 Pflops astrophysical N-body simulation on K computer—The gravitational trillion-body problem, arXiv:1211.4406.
[43] P. S. Behroozi, R. H. Wechsler, and H.-Y. Wu, The rockstar phase-space temporal halo finder and the velocity offsets of cluster cores, Astrophys. J. **762**, 109 (2013).
[44] P. S. Behroozi, R. H. Wechsler, H.-Y. Wu, M. T. Busha, A. A. Klypin, and J. R. Primack, Gravitationally consistent halo catalogs and merger trees for precision cosmology, Astrophys. J. **763**, 18 (2013).
[45] J. Diemand, M. Kuhlen, and P. Madau, Early supersymmetric cold dark matter substructure, Astrophys. J. **649**, 1 (2006).
[46] C. Giocoli, G. Tormen, R. K. Sheth, and F. C. van den Bosch, The substructure hierarchy in dark matter haloes, Mon. Not. R. Astron. Soc. **404**, 502 (2010).
[47] S. Ando and E. Komatsu, Constraints on the annihilation cross section of dark matter particles from anisotropies in the diffuse gamma-ray background measured with Fermi-LAT, Phys. Rev. D **87**, 123539 (2013).
[48] J. Zavala and N. Afshordi, Universal clustering of dark matter in phase space, Mon. Not. R. Astron. Soc. **457**, 986 (2016).
[49] Á. Moliné, M. A. Sánchez-Conde, S. Palomares-Ruiz, and F. Prada, Characterization of subhalo structural properties and implications for dark matter annihilation signals, Mon. Not. R. Astron. Soc. **466**, 4974 (2017).
[50] M. A. Sánchez-Conde and F. Prada, The flattening of the concentration-mass relation towards low halo masses and its implications for the annihilation signal boost, Mon. Not. R. Astron. Soc. **442**, 2271 (2014).
[51] M. Kamionkowski and S. M. Koushiappas, Galactic substructure and direct detection of dark matter, Phys. Rev. D **77**, 103509 (2008).
[52] M. Kamionkowski, S. M. Koushiappas, and M. Kuhlen, Galactic substructure and dark matter annihilation in the Milky Way Halo, Phys. Rev. D **81**, 043532 (2010).
[53] M. Stref and J. Lavalle, Modeling dark matter subhalos in a constrained galaxy: Global mass and boosted annihilation profiles, Phys. Rev. D **95**, 063003 (2017).
[54] C. Okoli and N. Afshordi, Concentration, ellipsoidal collapse, and the densest dark matter haloes, Mon. Not. R. Astron. Soc. **456**, 3068 (2016).
[55] M. Gosenca, J. Adamek, C. T. Byrnes, and S. Hotchkiss, 3D simulations with boosted primordial power spectra and ultracompact minihalos, Phys. Rev. D **96**, 123519 (2017).
[56] M. S. Delos, A. L. Erickcek, A. P. Bailey, and M. A. Alvarez, Are ultracompact minihalos really ultracompact?, Phys. Rev. D **97**, 041303 (2018).
[57] M. Ackermann *et al.* (Fermi-LAT Collaboration), The spectrum of isotropic diffuse gamma-ray emission between 100 MeV and 820 GeV, Astrophys. J. **799**, 86 (2015).
[58] M. Ackermann *et al.* (Fermi-LAT Collaboration), Limits on dark matter annihilation signals from the Fermi LAT 4-year measurement of the isotropic gamma-ray background, J. Cosmol. Astropart. Phys. 09 (2015) 008.
[59] G. Steigman, B. Dasgupta, and J. F. Beacom, Precise relic WIMP abundance and its impact on searches for dark matter annihilation, Phys. Rev. D **86**, 023506 (2012).
[60] S. Ando, Gamma-ray background anisotropy from galactic dark matter substructure, Phys. Rev. D **80**, 023520 (2009).
[61] I. Cholis and D. Hooper, Constraining the origin of the rising cosmic ray positron fraction with the boron-to-carbon ratio, Phys. Rev. D **89**, 043013 (2014).
[62] M. Di Mauro and F. Donato, Composition of the Fermi-LAT isotropic gamma-ray background intensity: Emission from extragalactic point sources and dark matter annihilations, Phys. Rev. D **91**, 123001 (2015).
[63] A. Albert *et al.* (DES and Fermi-LAT Collaborations), Searching for dark matter annihilation in recently discovered

Milky Way satellites with Fermi-LAT, Astrophys. J. **834**, 110 (2017).
[64] M. Hütten, C. Combet, and D. Maurin, Extragalactic diffuse γ-rays from dark matter annihilation: Revised prediction and full modelling uncertainties, J. Cosmol. Astropart. Phys. 02 (2018) 005.
[65] M. Fornasa *et al.*, Angular power spectrum of the diffuse gamma-ray emission as measured by the Fermi Large Area Telescope and constraints on its dark matter interpretation, Phys. Rev. D **94**, 123005 (2016).
[66] S. Ando and E. Komatsu, Anisotropy of the cosmic gamma-ray background from dark matter annihilation, Phys. Rev. D **73**, 023521 (2006).
[67] S. Ando, E. Komatsu, T. Narumoto, and T. Totani, Dark matter annihilation or unresolved astrophysical sources? Anisotropy probe of the origin of cosmic gamma-ray background, Phys. Rev. D **75**, 063519 (2007).
[68] S. Ando, M. Fornasa, N. Fornengo, M. Regis, and H.-S. Zechlin, Astrophysical interpretation of the anisotropies in the unresolved gamma-ray background, Phys. Rev. D **95**, 123006 (2017).
[69] S. Ando, A. Benoit-Lévy, and E. Komatsu, Mapping dark matter in the gamma-ray sky with galaxy catalogs, Phys. Rev. D **90**, 023514 (2014).
[70] S. Ando, Power spectrum tomography of dark matter annihilation with local galaxy distribution, J. Cosmol. Astropart. Phys. 10 (2014) 061.
[71] N. Fornengo and M. Regis, Particle dark matter searches in the anisotropic sky, Front. Phys. **2**, 6 (2014).
[72] M. Lisanti, S. Mishra-Sharma, N. L. Rodd, and B. R. Safdi, A search for dark matter annihilation in galaxy groups, Phys. Rev. Lett. **120**, 101101 (2018).
[73] A. D. Ludlow, S. Bose, R. E. Angulo, L. Wang, W. A. Hellwing, J. F. Navarro, S. Cole, and C. S. Frenk, The mass-concentration-redshift relation of cold and warm dark matter haloes, Mon. Not. R. Astron. Soc. **460**, 1214 (2016).